Compressive Strength of UHPC in Bottle-Shaped Compression Fields

Torsten Leutbecher, Ekkehard Fehling
Institute of Structural Engineering, University of Kassel, Germany

To investigate the load-bearing behavior in bottle-shaped compression fields, an extensive test program has been initiated including series on ultra high performance concrete (UHPC) as well as on high strength (HSC) and normal strength concrete (NSC). In bottle-shaped compression fields transverse compressive stresses arise directly below the concentrated load while tensile stresses act at a slightly larger distance from the load introduction area. The tensile strength may limit the bearing capacity if there is no transverse reinforcement. The experimental tests, presented in the following, showed that splitting was the governing failure mode in all cases. The fracture behavior was brittle for UHPC and HSC specimens without fibers. By using fibers, the load bearing capacity could be increased significantly. Also a more ductile behavior at ultimate load could be observed.

Keywords: bottle-shaped, stress field, biaxial, tension, compression, concentrated load, splitting

1 Introduction

Applying a concentrated load to a structural concrete member often results in a bottle-shaped compression field in the load introduction zone (see Fig. 1). By deflecting the stress trajectories, compressive stresses arise in transverse direction at the bottle neck (directly below the concentrated load) and tensile stresses in a slightly larger distance from the load introduction area. A typical example for the formation of a bottle-shaped compression field is the introduction zone of the pre-stressing force in pre-stressed concrete structures.

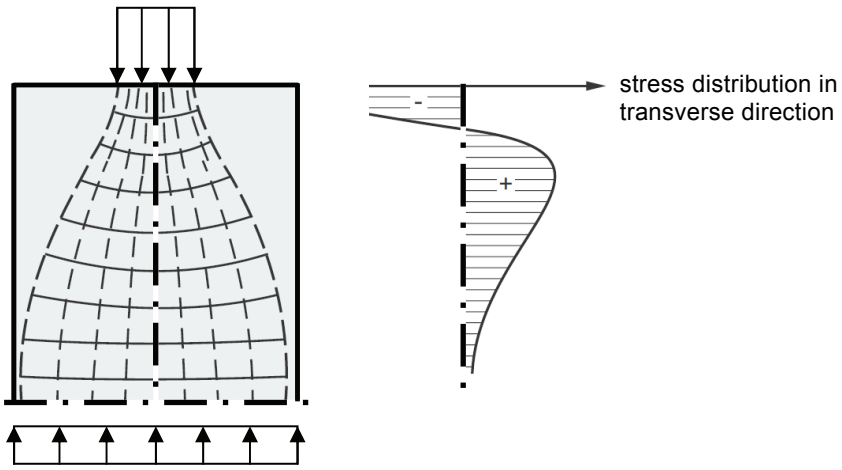

Figure 1: Bottle-shaped compression field under concentrated loads

Usually, the transverse tensile stresses in structural concrete members are covered by transverse reinforcement. If this is not wanted or not possible, the compressive stresses under the concentrated load normally have to be limited to ensure that transverse tensile stresses do not exceed the value of the concrete tensile strength. An application is the use of high strength and ultra high strength concrete for so-called grouted connections in offshore power plants.

In these connections, the concrete makes it possible to transmit the load between the steel foundation pile(s) driven into the seabed and the upper steel structure of the tower (see Fig. 2). Compared to a pure steelwork connection, the grouting of the annular gap between these two parts with (ultra) high strength concrete offers the advantage of an easier compensation of

tolerances (especially deviations of the pile relative to the vertical axis). To prevent slippage in cylindrical connections, so-called shear keys are used. They are usually designed as circumferential weld beads. Besides the dead load, a part of the bending moment caused by wind and wave loads may be split into a couple of vertical forces and carried by the shear keys. The introduction of the concentrated forces from the steel tube into the concrete via shear keys results in a bottle-shaped compression field in the grouted connection. The question of designing these connections was responsible for initiating a test program, that is presented in the following.

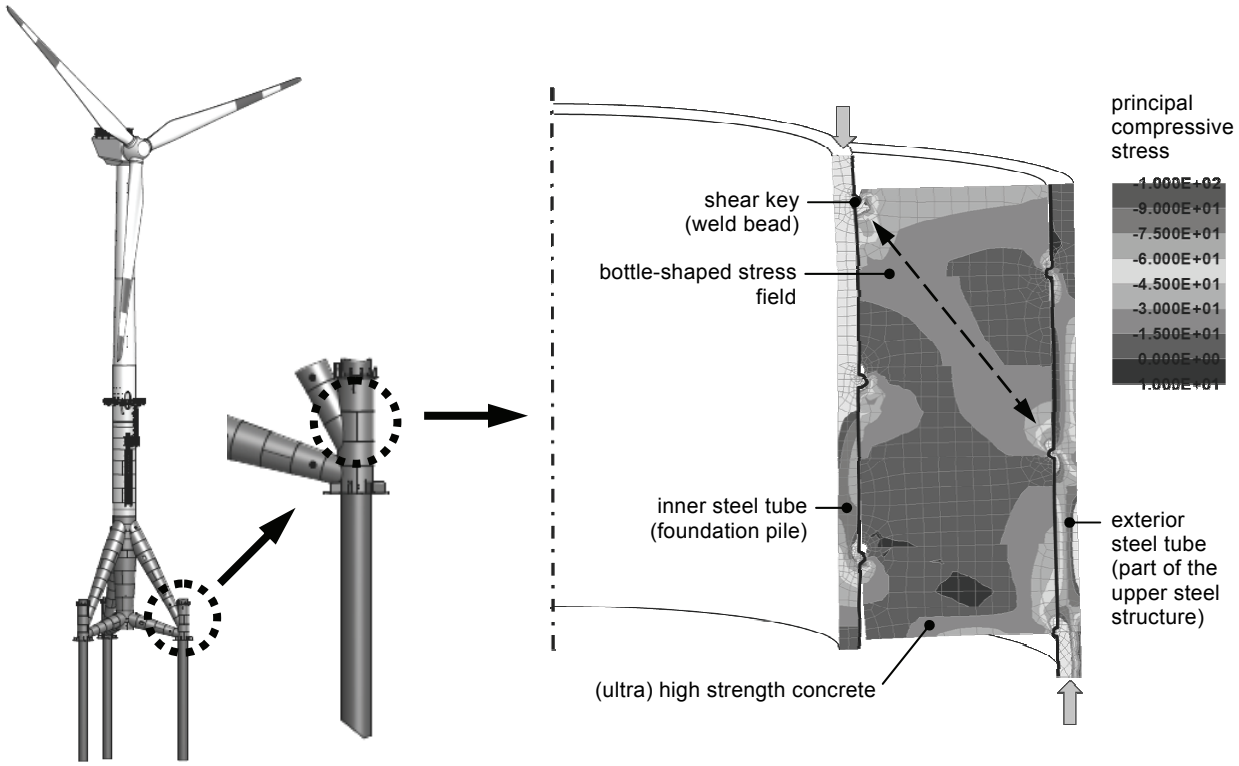

Figure 2: Offshore power plant of the wind farm Global Tech I in the Northern Sea (on the left) and FE-model of the grouted connection (on the right)

2 Cracking load of two-dimensional bottle-shaped compression fields

According to *Schlaich* and *Schäfer* [1], the cracking load represents a lower limit of the load-bearing capacity of two-dimensional bottle-shaped compression fields. The cracking forces can be determined by linear-elastic analysis using finite elements for plane stress state. It should be noted that the cracking stress may differ from the uniaxial tensile strength as a result of the biaxial tension-compression stress state within the compression field.

In Fig. 3a *Schlaich* and *Schäfer* provide a diagram for the determination of the compressive load leading to cracking of bottle-shaped compression fields. The compression field is characterized by the width *a* of the concentrated load, the maximum width *b* that is available for the compression field in the structural member, and the distance *l* between the load introduction and the section in which the stress trajectories run parallel. For structural members with very large or unlimited width, the total width *b* is to be replaced by the effective width b_{ef} according to Fig. 4 when evaluating the diagram. This takes into account that the compressive stresses acting on half-height of the compression field are not distributed equally along the total width.

As an example, the cracking load is calculated for the case that the uniaxial tensile strength f_{ct} is equal to 1/15 of the uniaxial compressive strength of the concrete f_c and for a failure criterion under tension-compression loading according to Fig. 3c. The result is represented by

the thick solid line in Fig. 3a. The further graphs in Fig. 3a are obtained for compression fields with transverse reinforcement (see Fig. 3d) depending on the mechanical reinforcement ratio ω.

As experiments have shown, the actual failure load is often higher than the cracking load [2-4] due to redistribution of the tensile stresses over the height of the compression field.

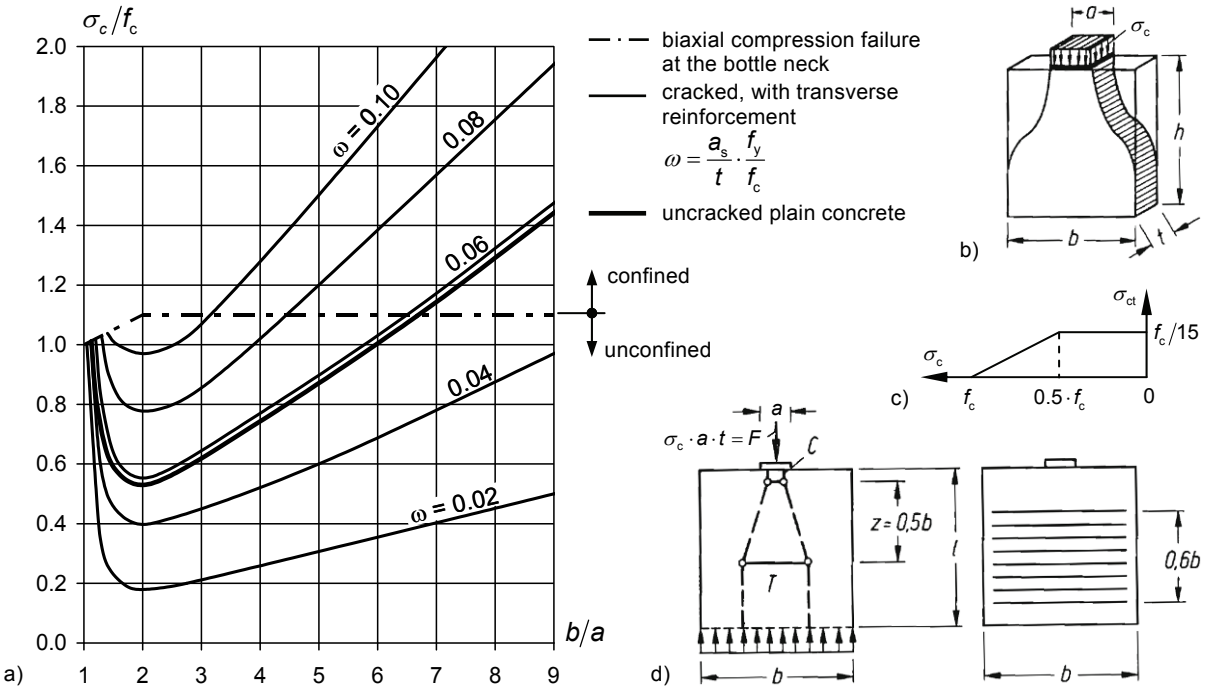

Figure 3: Two-dimensional bottle-shaped compression field according to Schlaich and Schäfer [1]
a) Compressive stress under the concentrated load causing a splitting crack (plain concrete, thick line), yielding of transverse reinforcement (thin lines) or biaxial compression failure at the bottle neck (dash-dotted line)
b) Geometry of the compression field
c) Failure criterion under biaxial tension-compression loading
d) Strut-and-tie model for the compression field with transverse reinforcement

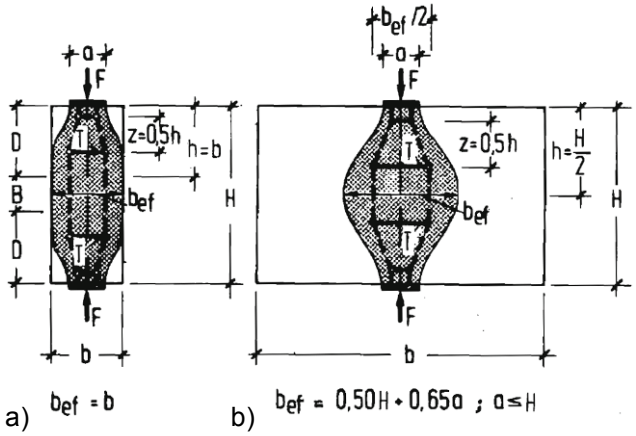

Figure 4: Effective width b_{ef} of the bottle-shaped compression field according to Schlaich and Schäfer [1]
a) structural member with small width
b) structural member with very large or unlimited width

3 Experimental investigations

Test program and test specimens

On the one hand, high strength (HSC) and ultra high performance concretes (UHPC) differ from normal-strength concretes (NSC) in increased brittleness and mostly in the use of a relatively small maximum aggregate size. On the other hand, steel fibers, which can act as “transverse reinforcement” in bottle-shaped compression fields, are often added, especially to UHPC.

To investigate the abovementioned influences on the bearing-capacity of bottle-shaped compression fields, tests on concrete cubes with different compressive strengths were conducted. Table 1 gives an overview of the experimental program executed so far.

Table 1: Test program executed so far

Test series	**NSC-0**	**HSC-0**	**UHPC-0-HT**	**UHPC-1-HT**	**UHPC-2-HT**
Uniaxial concrete compressive strength f_c [N/mm²]	19.7	131	194	200	201
Gross density [kg/dm³]	2.087	2.424	2.314	2.417	2.418
Maximum aggregate size [mm]	8	5	0.5	0.5	0.5
Fiber content ρ_f [% by vol.]	0	0	0	1.0	2.0
Heat treatment	no	no	yes	yes	yes

As fiber reinforcement straight steel fibers with a length of 17 mm and a diameter of 0.175 mm were used. They were added to two of the UHPC-mixtures with 1.0 % or 2.0 % by volume.

The concrete cubes had an edge length of 200 mm. They were produced in a steel mold and compacted on a vibrating table. To compact the NSC specimens, an internal vibrator was used. For each test series four concrete cubes and three cylinders (h/d = 200 mm/100 mm) were fabricated from the same mixture. The cylinders were used to determine the uniaxial concrete compressive strength. The NSC and HSC specimens were cured under room conditions after removing the formwork two days after production. The UHPC series were heat treated (labeled HT) at 90 °C for 48 hours with the result that the final strength of these specimens was achieved at the age of four days.

Test setup und test execution

The experiments were conducted in a servo-hydraulic controlled universal testing machine in the laboratory of the Institute of Structural Engineering at the University of Kassel. Fig. 5 shows the test setup.

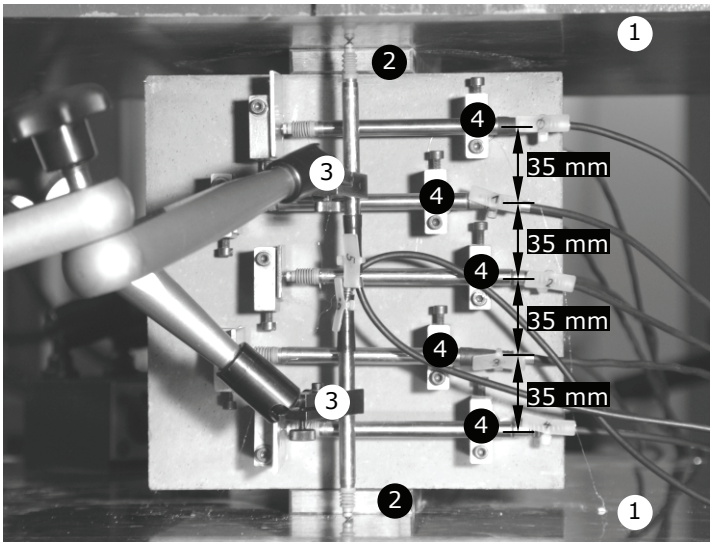

(1) Loading plates of the testing machine
(2) Steel stripes for load introduction (here: a = 60 mm)
(3) LVDTs for control of vertical displacements
(4) LVDTs for control of horizontal displacements

Figure 5: Test setup with test specimen and instrumentation

The test specimens were placed centrically between the two loading plates of the machine. The upper loading plate was connected via a spherical hinge to the testing machine. The specimens were loaded perpendicular to the casting direction. The load was applied by means

of 200 mm long steel strips, which were placed centrically at the top and at the bottom of the test specimen. Because of the smooth concrete surface obtained by the steel mold, the steel strips could be installed without any interface layer. To obtain different geometries of the compression field b/a, steel strips with four different width values were used for load introduction (a = 10 mm, 16 mm, 25 mm, and 60 mm). This resulted in ratios $b_{(ef)}/a$ of 10.7, 6.9, 4.7, and 2.3. Hence, each ratio was applied to one of the cubes of each series.

To measure the deformations in compression direction, four LVDTs were installed, two at the front and two at the back side of the cube. They were fixed with magnetic stands and measured against the load plates of the testing machine. In addition, the displacement of the hydraulic jack was recorded.

The horizontal deformations (in tensile direction) were checked in the area in which cracking could be expected. They were measured directly by means of LVDTs mounted on the specimen. At the front and the back of the specimens five gauge lengths of 100 mm were provided. For some specimens without fibers, two gauge lengths remained vacant on each side, because it was already known from previous experiments, that meaningful data could not be gained from these specimens in the post-cracking branch due to the brittle failure.

Displacement controlled loading was performed with a constant rate of 0.01 mm/s (displacement of the hydraulic jack).

Test results

The test results are summarized in Table 2. The ultimate compressive stresses $\sigma_{c,max}$ are related to the load application area represented by the surface area of the steel strip. As expected, the ratio $\sigma_{c,max}/f_c$ increases with increasing ratio b/a. The ratio decreases significantly with increasing uniaxial concrete compressive strength f_c due to the minor ratio between tensile and compressive strength and the more pronounced brittleness of HSC and UHPC.

Table 2: Test results

Test series	NSC-0		HSC-0		UHPC-0-HT		UHPC-1-HT		UHPC-2-HT	
	$\sigma_{c,max}$ [N/mm²]	$\sigma_{c,max}/f_c$	$\sigma_{c,max}$ [N/mm²]	$\sigma_{c,max}/f_c$	$\sigma_{c,max}$ [N/mm²]	$\sigma_{c,max}/f_c$	$\sigma_{c,max}$ [N/mm²]	$\sigma_{c,max}/f_c$	$\sigma_{c,max}$ [N/mm²]	$\sigma_{c,max}/f_c$
b/a = 2.3	17.6	0.89	79.4	0.61	78.9	0.41	173	0.87	193	0.96
b/a = 4.7	23.2	1.18	77.2	0.59	74.2	0.38	207	1.04	284	1.41
b/a = 6.9	34.6	1.75	95.3	0.73	109	0.56	256	1.28	334	1.66
b/a = 10.7	48.9	2.48	151	1.15	158	0.81	347	1.73	457	2.27

For some tests, the load-deformation curves are depicted in Fig. 6. All deformations specified in the diagrams represent mean values of the data obtained at the front and at the back side of the test specimens. In vertical direction, the elastic deformations of the steel stripes have been deducted.

Fig. 6a and 6b show the load-deformation curves for the ratio b/a = 10.7. Disregarding some nonlinearities resulting from the test setup, the load-deformation behavior of the test specimens was initially linear both in loading and transverse direction.

The HSC specimens and the UHPC specimens without fibers failed suddenly by a splitting crack (see Fig. 7c) accompanied by a load drop to zero in most cases. Also the NSC cubes did not show a pronounced nonlinear behavior before reaching the ultimate load. However, for these specimens the complete softening branch after splitting could be obtained by displacement control.

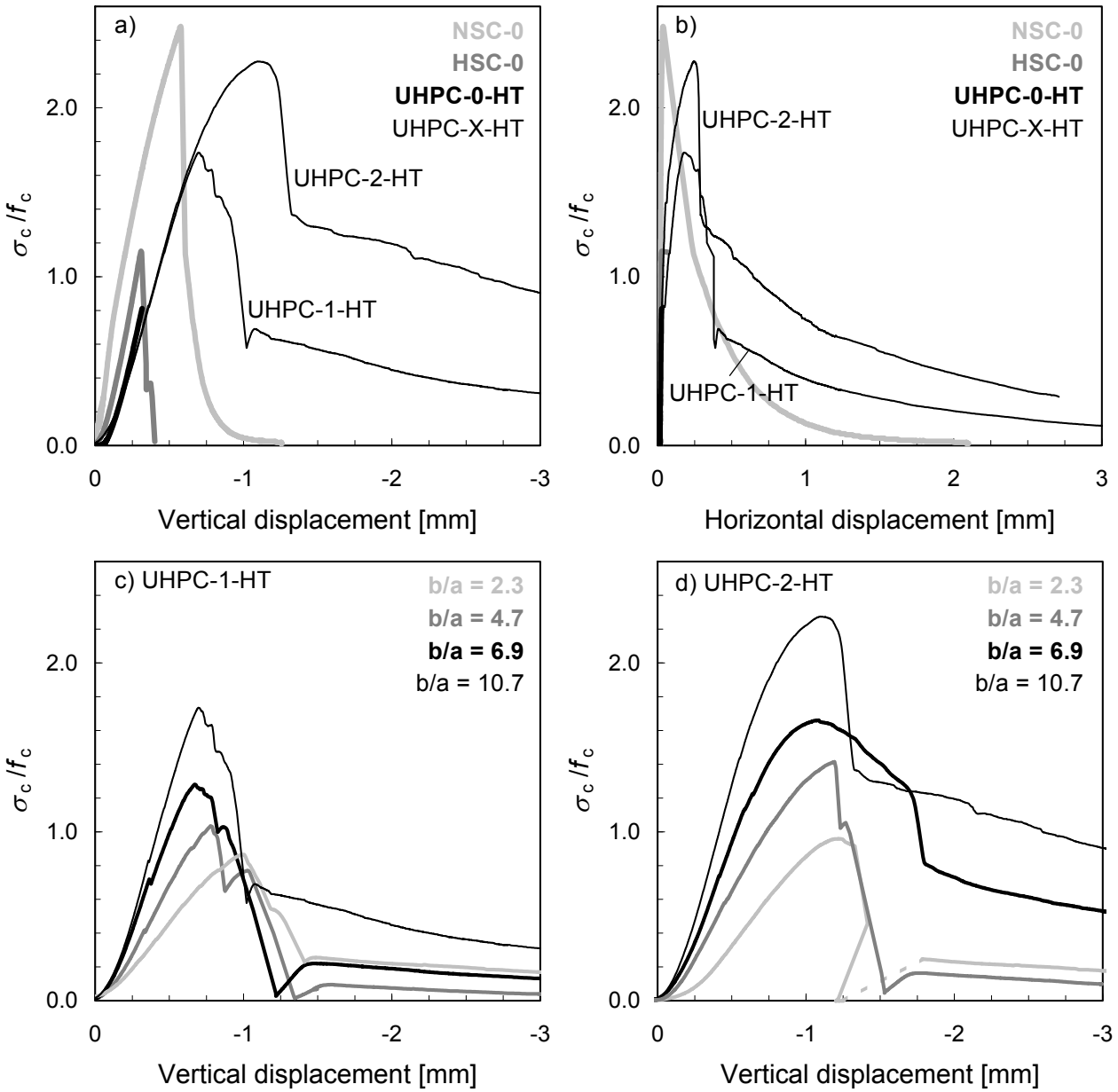

Figure 6: Load-deformation curves
a) Load-deformation curve in loading (compression) direction for the five series and b/a = 10.7.
b) Load-deformation curve in transverse (tension) direction for the five series and b/a = 10.7.
c) Load-deformation curve in loading (compression) direction for series UHPC-1-HT and different ratios b/a
d) Load-deformation curve in loading (compression) direction for series UHPC-2-HT and different ratios b/a

For the fiber reinforced UHPC cubes, the load-deformation relationship initially followed almost that of the corresponding unreinforced specimens. The splitting started at about the same load level, too. However, this caused only a temporary slight drop of the load. With increasing deformation, the compressive load could be further increased, while henceforth a nonlinear relationship between load and deformation was observed. The progressive crack opening could be detected by the horizontal LVDTs very well (see Fig. 6b). The failure was announced by more or less pronounced plastic behavior before reaching the ultimate load. The specimens with large *b*/*a* ratio and higher fiber content showed in this context as well as in the post-peak branch a more ductile behavior (see Fig. 6c and 6d). For small *b*/*a* ratios the loading dropped comparatively rapidly to zero, even for the specimens with a fiber content of 2 % by volume.

Fig. 7 shows the failure pattern of split UHPC specimens. For the specimens with b/a = 2.3, splitting started from the edges of the load application area due to load concentration there. As a consequence sometimes two splitting cracks developed (see Fig. 7a).

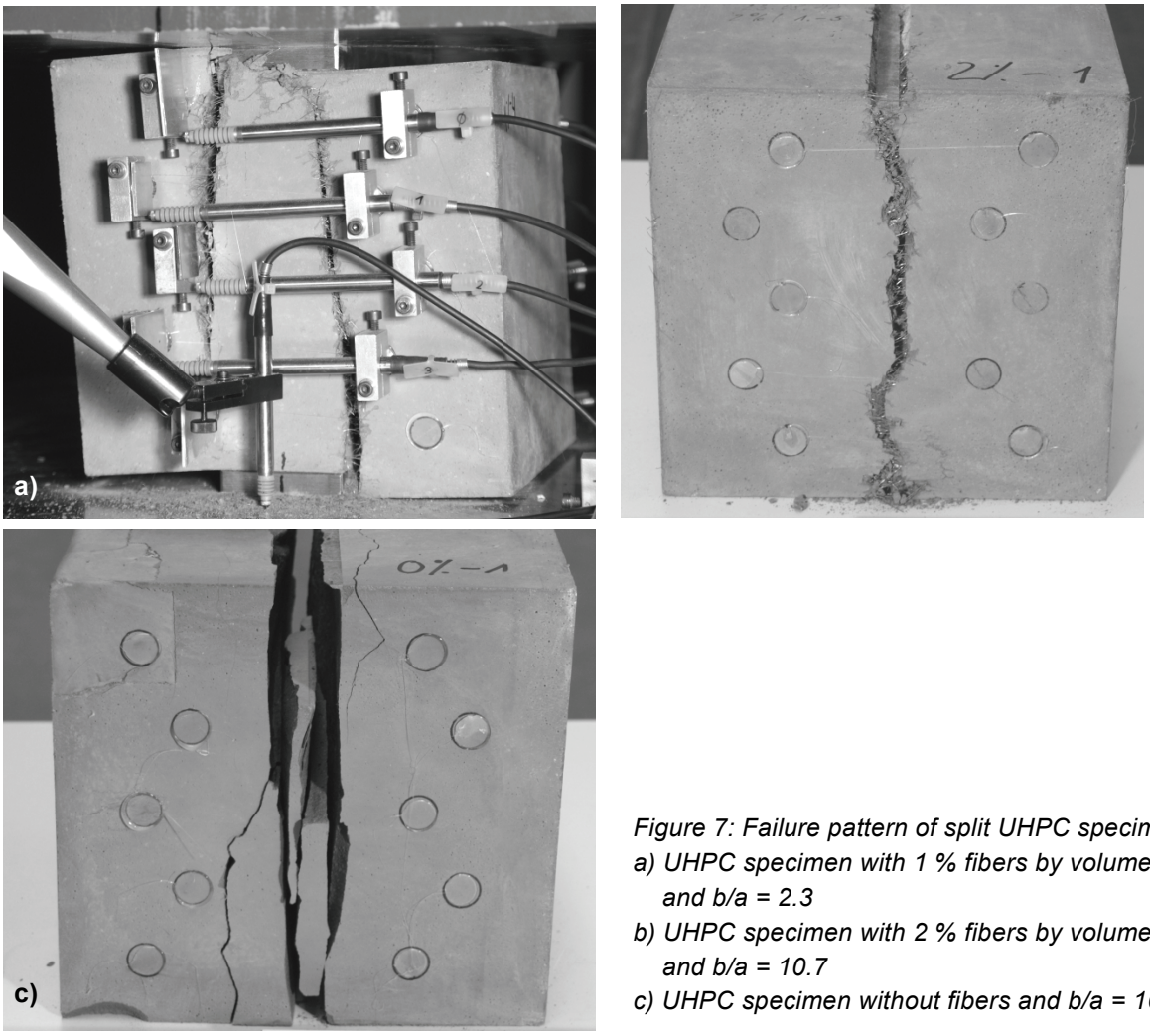

Figure 7: Failure pattern of split UHPC specimens
a) UHPC specimen with 1 % fibers by volume and b/a = 2.3
b) UHPC specimen with 2 % fibers by volume and b/a = 10.7
c) UHPC specimen without fibers and b/a = 10.7

4 Conclusions and outlook

Fig. 8 shows the ultimate compressive stresses due to concentrated load, which are related to the uniaxial concrete compressive strength. The results are depicted in dependency of the theoretical b/a ratio.

The results for the NSC specimens can be approximately related to ω = 0.09. This corresponds to a ratio between the concrete tensile strength f_{ct} and the uniaxial concrete compressive strength f_c of about 1/10, which is common for NSC. Referring the results for the HSC and UHPC specimens to the graphs ω = 0.04 and ω = 0.03, respectively, the ratios f_{ct}/f_c amount to about 1/22 and 1/29. For uniaxial compressive strengths of 131 N/mm² and 194 N/mm², respectively, the tensile strengths result in about 6.0 N/mm² and 6.7 N/mm².

By means of fiber addition to UHPC the load bearing capacity could be increased significantly. Already a fiber volume of 1 % was sufficient to achieve compressive stresses under the concentrated load that were almost equal to the uniaxial concrete compressive strength. Compared to the ultimate load, the ductility was increased at a lower rate by the addition of fibers, especially for the specimens with low b/a ratio. Despite the sometimes very high local stresses at the steel strip, splitting and not compression failure was governing in all cases.

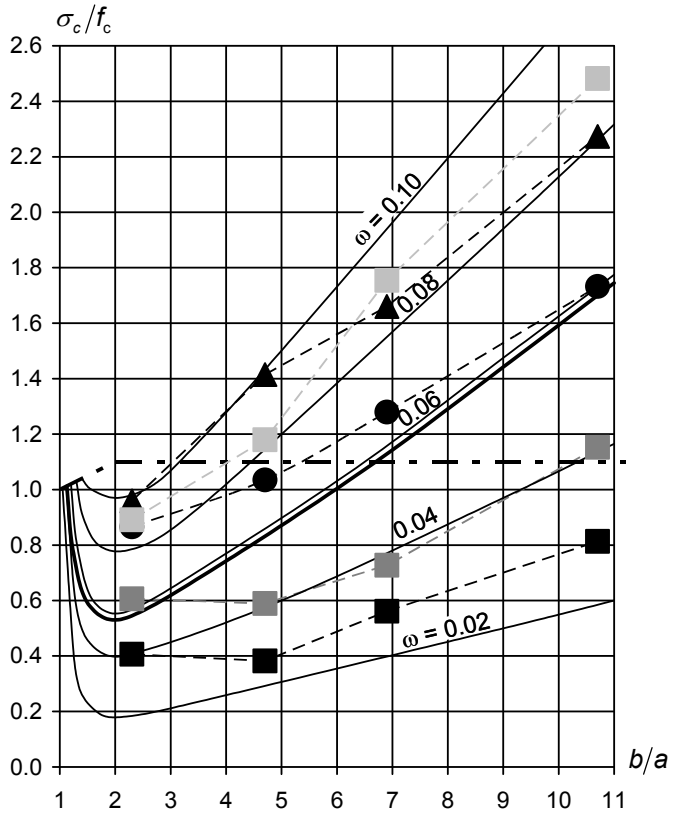

Figure 8: Test results related to the uniaxial concrete compressive strength and compared with the theoretical cracking stress according to [1] (see Fig. 3)

Further tests on HSC with fibers as well as on UHPC with low fiber content (0.5 % by volume) are scheduled. By optically analyzing the fiber orientation in the cubes and by determining the post-cracking tensile strength (fiber efficiency) in tests on notched prisms sawn from untested cubes, a relationship to concretes with different fiber content and fiber geometry may be established. The test results will also be used to calibrate a fracture model for fiber reinforced UHPC within a nonlinear finite element analysis. Afterwards, this model shall be applied to the design of grouted connections used in offshore wind turbines. For this, the fracture model is to be extended so that it is appropriate for three-dimensional stress states.

References

[1] Schlaich, J.; Schäfer, K.: Konstruieren im Stahlbetonbau. Beton-Kalender 1998, part II, Verlag Ernst & Sohn, Berlin, 1998.

[2] Fehling, E.: Zum Tragverhalten von Druckfeldern in scheibenartigen Betonbauteilen - Nichtlineare Berechnungen und Vergleich mit Versuchen. Materialmodelle und Methoden zur wirklichkeitsnahen Berechnung von Beton-, Stahlbeton- und Spannbetonbauteilen, Mehlhorn-Festschrift, Faculty of Civil Engineering, University of Kassel, 1997.

[3] Colombo, M.; Di Prisco, M.: D-zones in HPFRC. High Performance Fiber Reinforced Cement Composites 6 (Eds.: Parra-Montesinos, G. J.; Reinhardt, H. W.; Naaman; A. E.), Proceedings of the Sixth International Workshop on High Performance Fiber Reinforced Cement Composites (HPFRCC6), pp. 197-204, Ann Arbor, MI, USA, 2011.

[4] Pujol, S.; Rautenberg, J. M.; Sozen, M. A.: Compressive Strength of Concrete in Nonprismatic Elements. *Concrete International* 33 (9), pp. 42-49, 2011.